View metadata, citation and similar papers at core.ac.uk

brought to you by CORE

provided by Missouri University of Science and Technology (Missouri S&T): Scholars' Mine

Missouri University of Science and Technology

Scholars' Mine

International Specialty Conference on Cold-Formed Steel Structures

(2014) - 22nd International Specialty Conference on Cold-Formed Steel Structures

Nov 5th, 12:00 AM - 12:00 AM

Laser Scanning to Develop Three-Dimensional Fields for the Precise Geometry of Cold-Formed Steel Members

Xi Zhao

Benjamin W. Schafer

Follow this and additional works at: https://scholarsmine.mst.edu/isccss

 Part of the Structural Engineering Commons

Recommended Citation

Zhao, Xi and Schafer, Benjamin W., "Laser Scanning to Develop Three-Dimensional Fields for the Precise Geometry of Cold-Formed Steel Members" (2014). *International Specialty Conference on Cold-Formed Steel Structures*. 7.
https://scholarsmine.mst.edu/isccss/22iccfss/session01/7

This Article - Conference proceedings is brought to you for free and open access by Scholars' Mine. It has been accepted for inclusion in International Specialty Conference on Cold-Formed Steel Structures by an authorized administrator of Scholars' Mine. This work is protected by U. S. Copyright Law. Unauthorized use including reproduction for redistribution requires the permission of the copyright holder. For more information, please contact scholarsmine@mst.edu.

Twenty-Second International Specialty Conference on Cold-Formed Steel Structures
St. Louis, Missouri, USA, November 5 & 6, 2014

Laser scanning to develop three-dimensional fields for the precise geometry of cold-formed steel members

Xi Zhao[1], Benjamin W. Schafer [2]

Abstract

Geometric imperfections play an important role in the performance and behavior of cold-formed steel members. The objective of this paper is to detail a newly developed imperfection measurement rig, where the full three-dimensional (3D) imperfect geometry of a cold-formed steel member can be measured and reconstructed. The measurement results in a dense three-dimensional point cloud that may be utilized to provide precise knowledge of the basic member dimensions (width, angle, radius including variation along the length), frequency content in the member (waviness, local dents, etc.), or directly as the exact geometry of the member. Practical applications of the data include basic quality control; however, the potential of the data is truly realized when applied to shell finite element models of cold-formed steel members to investigate imperfection sensitivity. The measurement rig set-up (Phase I) consists of three basic parts: a two-dimensional (2D) laser scanner with measurement range up to 304 mm [12 in.]; a linear drive system, allowing the laser to collect measurements of cross sections along the length of the target specimen; and a support beam. The raw point cloud data from the Phase I rig is input into MATLAB where custom post-processing is employed to develop the full 3D reconstruction of the target specimen. The Phase II rig adds a rotary ring, providing a rotational stage for the laser so that the cross section of the target specimen may be profiled from any direction. This paper provides several examples of full-field imperfection measurements and compares against other methods in current use. The measured imperfections contribute to the database of realized imperfections appropriate for the generation of stochastic imperfections for use in simulation. Accurate knowledge of geometric imperfections is critical to the long-term success of analysis-based design paradigms for cold-formed steel.

[1] Research Assistant, Johns Hopkins University, Baltimore, MD, 21218, USA. (xzhao16@jhu.edu)
[2] Professor, Johns Hopkins University, Baltimore, MD, 21218, USA. (schafer@jhu.edu)

Introduction

Initial imperfection measurements have long been of interest for thin-walled shell applications, for example as utilized in aerospace structures. Initial imperfection measurement has a long history dating back to at least 1906, when Stewart developed an autographic measuring device to investigate the collapsing pressure of Bessemer steel lap-welded tubes (Steward,1906). A Caltech centered group in the 1970s, e.g., (Arbocz & Williams, 1977) and Delft (Netherlands) centered group in the 1980s e.g., (Sebek, 1981) carried out extensive and important imperfection surveys on large or full-scale cylindrical shells. Imperfection measurements implemented in most structural testing laboratories have followed these examples.

For shells, Koiter's work (Koiter, 1967) indicated that the observed strength degradation in shell strength, or the related "knock-down factor", depends on the magnitudes and shape of geometric imperfections. However, individual prototypes of imperfection from experiments cannot predict well the buckling load of thin-walled shells (Arbocz & Hol, 1991). Therefore, it is recommended to characterize initial imperfection distributions that a particular fabrication process is likely to produce, and then combine this influence with a statistical analysis of both the initial imperfection and the corresponding critical load (Chryssanthopoulos & Poggi, 1995).

For cold-formed steel members imperfections are also important. Zeinoddini (2012) summarizes the available data and carried out a large number of surveys on lipped channel sections. The measured data was characterized as five different imperfection modes, corresponding (sometimes only loosely) to five buckling modes: local buckling (d1), distortional buckling (d2), strong-axis flexural buckling (G1), weak-axis flexural buckling (G2), and torsional buckling (G3). Magnitudes of the different imperfection modes has been statistically analyzed and summarized. These magnitudes can be directly utilized in shell finite element models to investigate capacity, and imperfection sensitivity.

Conventional imperfection measurements utilizing LVDT-based contact-measurements cannot collect full cross section information. For example, the corners of the cross sections are a detail that is difficult to assess with current methods. In addition, the time consuming nature of current methods has resulted in the database being relatively small. High throughput methods are also needed for extending imperfection measurements out of the lab, and into the manufacturing facilities for quality control. All of these factors lead to an interest in full-field non-contact measurement for cold-formed steel members.,

Laser Scanning Methodology and Test Set-up

Non-contact measurement with an accuracy of at least 0.1 mm [0.005 in.] was selected as the desired measurement objective. This quickly lead to a focus on laser scanning technologies. Laser scanning applies triangulation and a source and receiver to achieve its measurement. For complete scanners, the laser head, consists of both a semi-conductor laser source and a light detector as shown in Figure 1. The detected signal is used to determine the relative distance to the target (Figure 1).

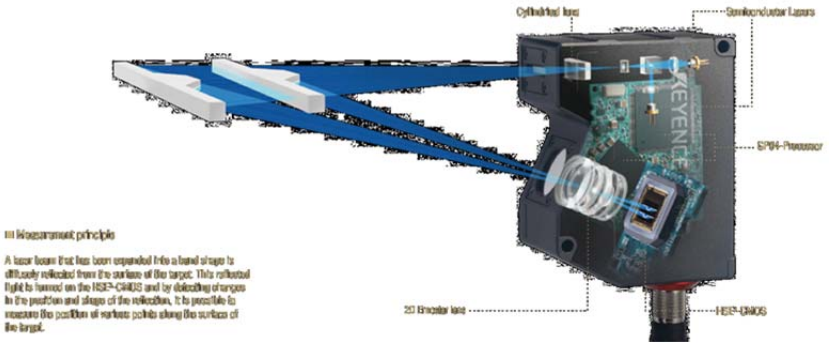

Figure 1 Laser triangulation and sensors (Keyence, 2012)

An imperfection measurement rig constructed by the first author, employing a line laser like that of Figure 1, is shown in Figure 2. This "Phase I" measurement rig is used for the data provided in this paper. The line laser is a Keyence LJ-V7300 and may profile a cross section up to 304 mm wide from 800 blue-light laser points. The short wavelength of the blue-light semi-conductor laser minimizes instrument error. The embedded double polarization program in the laser head helps eliminate stray reflections. The laser head is able to profile the target at high frequency (up to 16 kHz); therefore a linear drive system is employed in the measurement rig to readily scan along a the length of a target specimen by physically moving the laser head with the linear drive.

Target specimens are placed on the support beam facing the laser scanner as shown in Figure 3. For the lipped channel sections studied in this paper four sides, i.e. web, right flange, left flange and lips each must be scanned. Longitudinal position records are paired with the measured profiles for reconstruction of the 3D model. The resulting point clouds allow precise calculation of geometric imperfections.

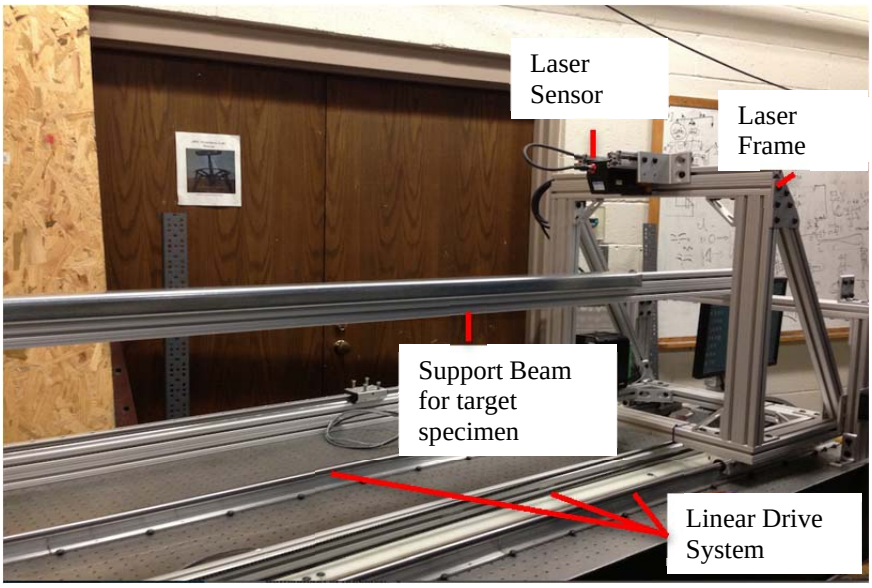

Figure 2 Phase I imperfection measurement rig

Figure 3 Detail of line laser measurement of the web of a specimen

Data Processing

Raw data format and pre-processing step
Raw data is stored in a csv file and read into MATLAB for processing The raw data contains invalid data (not of target) and noise from the set-up environment as shown in Figure 4. Pre-processing is carried out to remove most unwanted data, such as the support beams and other objects appearing in the scan not of interest..Further pre-processing is completed to change from the laser index to physical location (mm).

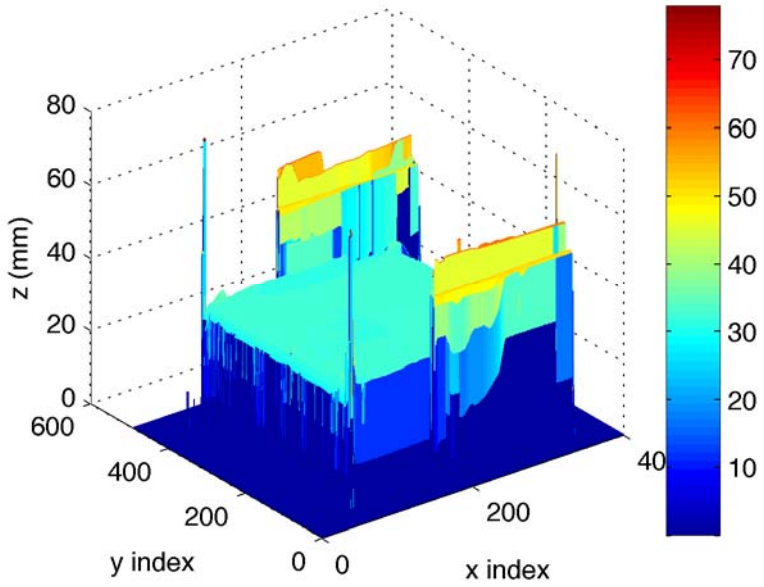

Figure 4 Raw data after a single scan

3D model reconstruction
The measured data from the web, right flange, left flange and lips (see Figure 5) must be stitched together to reconstruct the 3D model. This is completed based on three assumptions. *Assumption 1*: adjacent surfaces on the target share common laser measurement areas. For example, the scanned right flange overlaps with the scanned web of the target specimen at the corner. *Assumption 2*: All scanned surfaces share common longitudinal coordinates. *Assumption 3*: The specimen is perfectly supported by the measurement support beam, i.e. there is neither inclination about the z- nor x-direction in the reference frame.

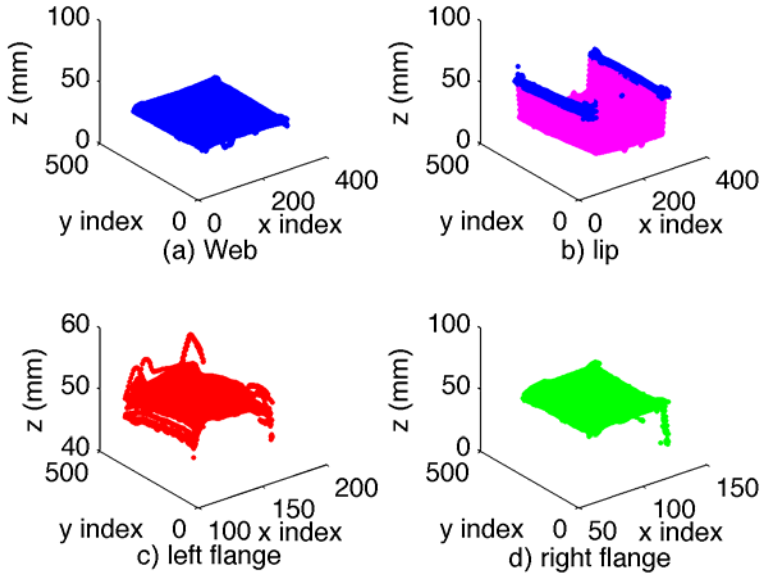

Figure 5 **Pre-processed data from four scans before stitching**

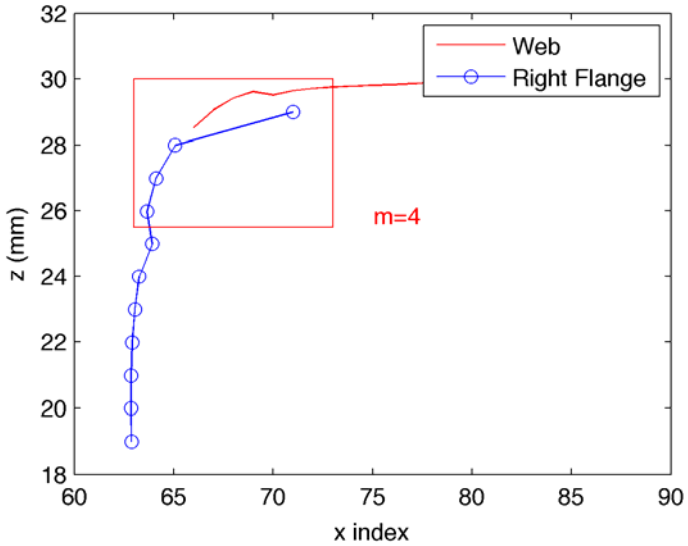

Figure 6 Conceptual picture of stitching two cross-sections

Based on the three assumptions above, model reconstruction is simplified to finding the in-plane translation and rotation to stitch the data. For a single section of the data the problem is illustrated in Figure 6: assuming the web as a reference, how should the right flange be translated and rotated to best match the overlapping points.

As an example consider the 4 surfaces scanned from a 48 in. long 600S137-54 [50ksi] (i.e. similar to Figure 5). A full scan contains 365 cross sections for a 4 ft long member. For the web and right flange, there are two sets of data $v_1 = \left(x_{ii}^{web}, z_{ii}^{web}\right)$ for the web and $v_2 = \left(x_j^{rf}, z_j^{rf}\right)$ for the right flange, where $ii = 1,2, \dots, k$ and $j = 1,2, \dots, n$. It is assumed that v_1 is invariant (the reference data) and v_2 may be adjusted by four varibles in a parameter vector β, defined by $\beta^T = [\beta_1, \beta_2, \beta_3, m]$, where β_1 is translation of $v_2$in *x*, β_2 is translation of v_2 in *z*, β_3 is rotation of v_2 in the x-z plane, and m is the number of overlapping points between v_1 and v_2 in a cross-section.

For a single cross-section with a given *m* the error function, S, which should be minimized to find β is given by Eq. 1:

$$S = \sum_{i=1}^{m} {r_i}^2 = \sum_{i=1}^{m} \{\left(z_i^{web} + \sin(\beta_3) x_j^{rf} - \cos(\beta_3)\, z_j^{rf} - \beta_2\right)^2 + \left(x_i^{web} - \cos(\beta_3) x_j^{rf} - \sin(\beta_3)\, z_j^{rf} - \beta_1\right)^2\} \quad (1)$$

The complete solution requires minimization over all N=365 cross-section, i.e.:

$$S = \sum_{k}^{N} \sum_{i=1}^{m} {r_{ik}}^2, \quad (2)$$

Assuming the number of overlapping points, *m*, is constant for a given stitching the best fit m is first found. Considering 30 random cross-sctions and empirically selecting a range for *m* per Table 1, the best fit S is found. As illustrated in Figure 7 error across the 30 samples varies, but is strongly correlated with the number of overlapping points, m. Considering mean S across the 30 samples, as provided in Figure 8, makes it clear that an optimal *m* can be achieved for a given stitching.

Table 1 Range of overlap points considered

Web & Flange	$m \in [2,8]$
Flange & Lips	$m \in [1,4]$

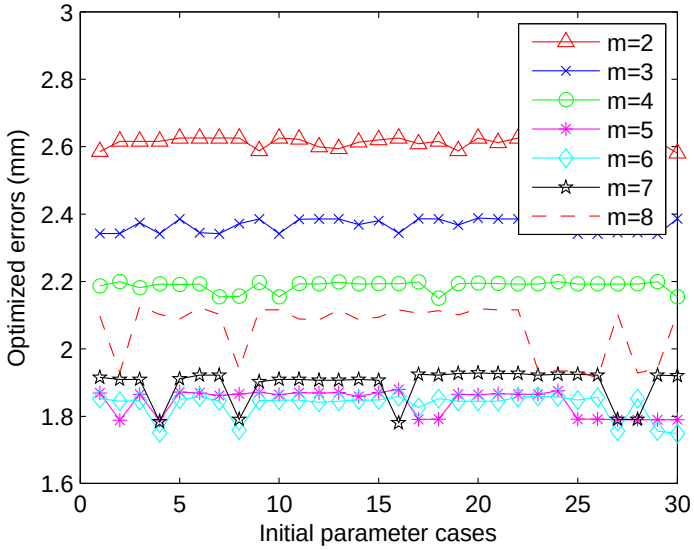

Figure 7 Minimized error for 30 cross-sections with different amount of assumed overlap (m)

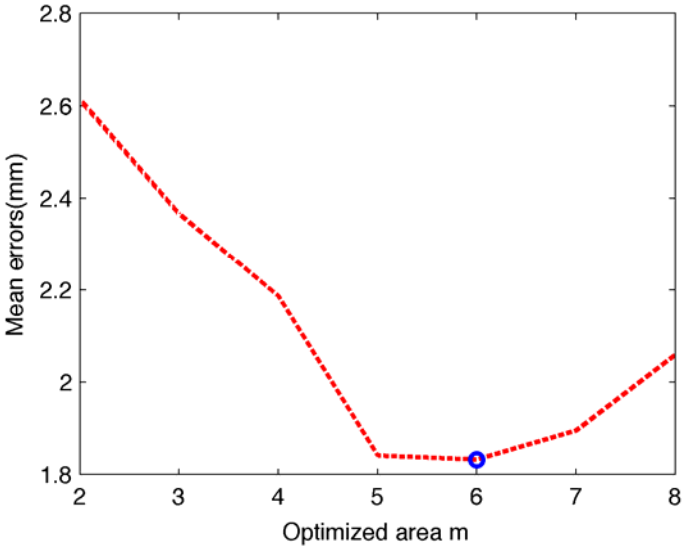

Figure 8 Example of selection for overlap, m, based on minimum error

With *m* selected, *S* of Eq. 2 is minimized resulting in the optimal stitching, as reported in Table 2 for this example. These parameters are applied to the corresponding surfaces resulting in the 3D model of Figure 9 and cross-sections, such as provided in Figure 10.

Table 2 Optimized parameter vector for S600-48-18 example

Stitching	$\boldsymbol{\beta_1}^{opt}$	$\boldsymbol{\beta_2}^{opt}$	$\boldsymbol{\beta_3}^{opt}$
	(mm)	(mm)	(deg.)
Web and Right Flange	- 21.5	16.5	2.64
Web and Left Flange	-127.7	23.4	1.85
Flanges and lips	- 7.9	26.9	-0.85

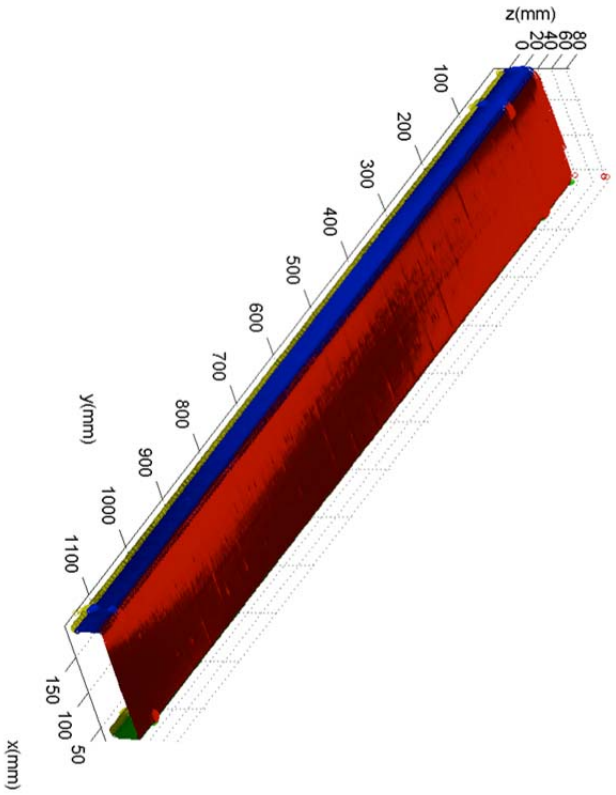

Figure 9 Reconstructed 3D model after stitching

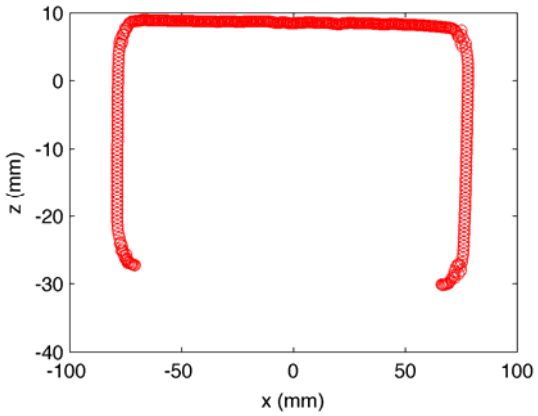

Figure 10 Typical cross-section from 3D reconstruction

Dimension and imperfection calculations

With the 3D point cloud reconstructed reduction of the data to dimensions, imperfections, etc. is now straightforward. Typical dimensions are illustrated in Figure 11. For example web height (H), flange width (B_1,B_2), and lip length (d_1, d_2) can be calculated via Eq. 3-5:

$$H = x_{right}^{web} - x_{left}^{web} \tag{3}$$

$$B_i = z_{top}^{flange} - z_{bot}^{flange}, i = 1,2 \tag{4}$$

$$d_i = x_{right}^{lip} - x_{left}^{lip}, i = 1,2 \tag{5}$$

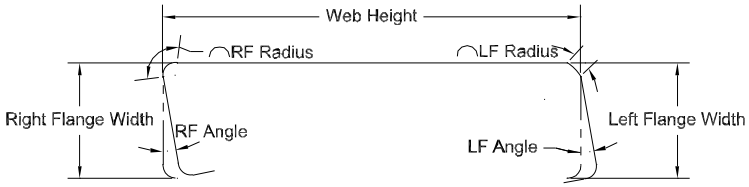

Figure 11 Notation for imperfect dimensions of specimen

The radius is slightly more involved, based on the determined overlap index *m*, points at the beginning, middle and end for calculating radius are extracted and the radius is then calculated as follows:

$$W = \sqrt{\left(x_{beg} - x_{end}\right)^2 + \left(z_{beg} - z_{end}\right)^2} \tag{6}$$

$$x_{int} = \frac{(z_{mid} - z_{beg}) - (s_2 x_{mid} - s x_{beg})}{s - s_2} \quad (7)$$

$$z_{int} = s_2(x - x_{mid}) + z_{mid} \quad (8)$$

$$s = \frac{z_{end} - z_{beg}}{x_{end} - x_{beg}} \text{ and } s_2 = -\frac{1}{s} \quad (9)$$

$$D = \sqrt{(x_{mid} - x_{int})^2 + (z_{mid} - z_{int})^2} \quad (10)$$

$$r = \frac{D}{2} + \frac{W^2}{8D} \quad (11)$$

The angles between the flanges and web can be calculated as follows:

$$s_1 = \frac{\left(z_{beg}^{flange} - z_{end}^{flange}\right)}{x_{beg}^{flange} - x_{end}^{flange}} \quad (12)$$

$$s_2 = \frac{\left(z_{beg}^{web} - z_{end}^{web}\right)}{x_{beg}^{web} - x_{end}^{web}} \quad (13)$$

$$\Delta s = s_2 - s_1 \quad (14)$$

$$\alpha = \tan^{-1} \Delta s \quad (15)$$

Global imperfections, Figure 12, i.e. bow (G1), camber (G2), and twist (G3), require estimating the imperfect centroid. This is done via:

$$x_c = \frac{\sum_{i=1}^{n} x_i^{flanges} + \sum_{i=1}^{m} x_i^{web} + \sum_{i=1}^{k} x_i^{lip}}{n+m+k} \quad (16)$$

$$z_c = \frac{\sum_{i=1}^{n} z_i^{flanges} + \sum_{i=1}^{m} z_i^{web} + \sum_{i=1}^{k} z_i^{lip}}{n+m+k} \quad (17)$$

From the centroids a straight line connecting the two ends is constructed and given as coordinates: (x_{perf}, z_{perf}). The difference between this straight line and the cross-section calculated centroids is a measure of the global imperfection (G1 and G2) along their length (in y), the maximum values are used as the imperfection magnitude, this is expressed as follows:

$$G1(y) = x_c - x_{perf} \quad (18)$$

$$G2(y) = z_c - z_{perf} \quad (19)$$

For G3, the cross sections at the beginning and end are assumed to be zero (i.e., they form the reference plane), then twist angle (γ) is estimated as follows:

$$s_i = \left(\frac{z_{left}^{web} - z_{right}^{web}}{x_{left}^{web} - x_{right}^{web}}\right)_i \quad (20)$$

$$\theta_i = \tan^{-1} s_i \quad (21)$$

$$\gamma_i = \theta_i - \theta_0 \quad (22)$$

where $i = 0,1, \ldots, N$

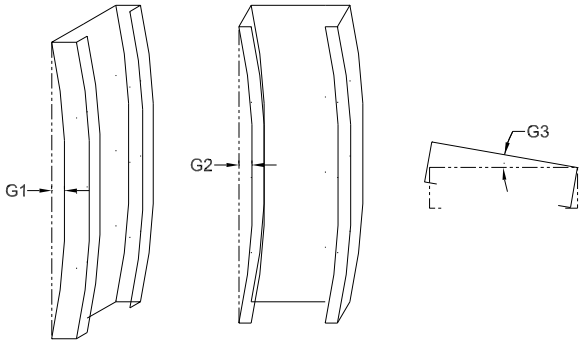

Figure 12 Global imperfections G1, G2, and G3

Plate (Type 1) and out-of-straigthness (Type 2) imperfecctions, Figure 13, may also be readily estimated from the data. Note, Type 1 imperfections are generally associated with local buckling and Type 2 with distortional buckling. Type 1 (local) imperfections are determined as the maximum perpendicular deviation from the perfect cross-section, within the web. Type 2 (distortional) imperfections are estimated as follows:

$$d2^{rf} = x_{end}^{right\ flange} - x_1^{right\ flange} \quad (23)$$

$$d2^{lf} = x_{end}^{left\ flange} - x_1^{left\ flange} \quad (24)$$

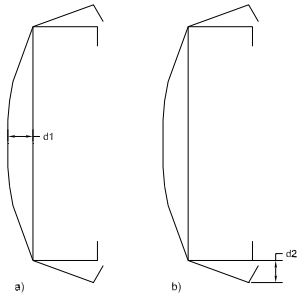

Figure 13 Type 1(a) and 2(b) imperfections (Schafer, 1997)

Example Study Results

Ten nominally identical 600S137-54 [50 ksi] cold-formed steel lipped channels, each 24 in. long, are selected for preliminary study. These sections are part of a separate experimental study on beam-columns. (Torabian et al. 2014).

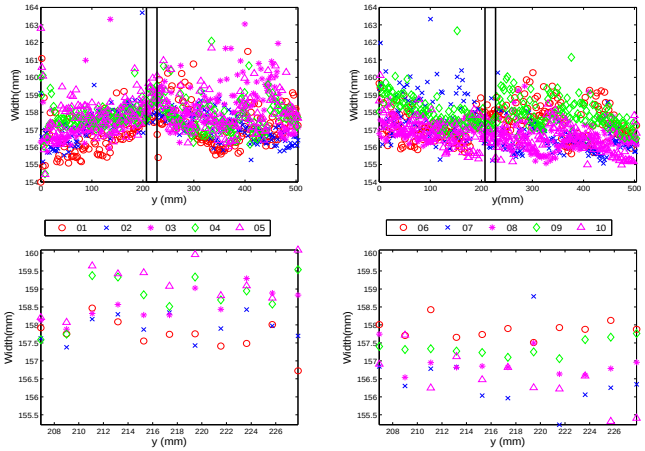

Figure 12 Web height along the specimen length for 10 specimens

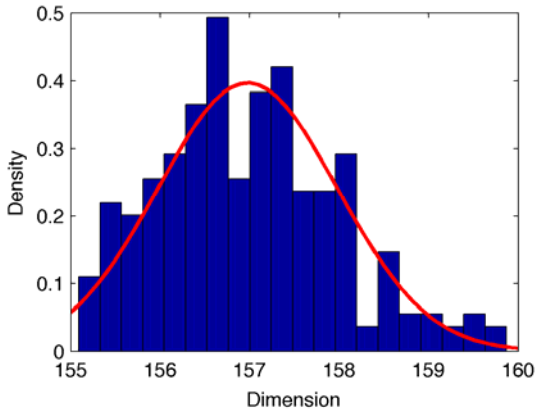

Figure 13 Scaled histogram and normal PDF for web height (mm)

Dimensions

The nominal out-to-out web depth (*H*) for the specimens is 152.4 mm; however, the actual web depth varies (with a mean of 157.2 mm across the samples). The ten samples are provided in Figure 14; not only does each sample vary, within

each specimen *H* also varies along the length, though the COV is small only about 0.5%. The data may be treated as a random process and the information from Figure 14 used to directly characterize the results, or more simply as a random variable, as shown in Figure 15. Similar characterizations can be provided for all the specimen dimensions – some indicate some interesting differences with nominal specifications: for example the mean outer corner radius is 6.4 mm compared with a nominal of 3.6 mm.

Global Imperfections

Global imperfections are assessed for the ten, 610mm [24 in.] long specimens. Typical variation along the length for bow, camber, and twist (G1, G2 and G3) are provided in Figure 16. The global imperfections generally follow a half-sine wave. Zeinoddini (2012) evaluated correlation between global imperfections and half-sine wave curves for data collected using contact measurements and concluded that global imperfections, particularly the G1 imperfection, is highly correlated with a sinusoid. Therefore, a half-sine wave can be accurately utilized as global imperfections in cold-formed steel modeling, magnitudes of which are statistically calculated in Zeinoddini (2011) for his data.

For the data studied here the maximum G1, G2, G3 is recorded for each specimen and provided in Table 3. The mean of these specimens is relatively high, approximately the 90^{th} percentile of the Zeinoddini (2011) data. This may be due to the specimen construction, which included welding at the ends which may exacerbate the global imperfections – further study is needed.

Table 3 Magnitudes of global imperfections

ID	**G1** (L/mag.)	**G2** (L/mag)	**G3** (deg/ft)
1	679	841	0.349
2	976	934	0.252
3	878	1072	0.171
4	1376	249	0.333
5	1262	156	0.509
6	1504	1273	0.409
7	448	762	0.331
9	499	3150	0.156
10	864	4137	0.391
11	2311	1213	0.252
mean	1080	1379	0.315
std. dev.	558	1269	0.109

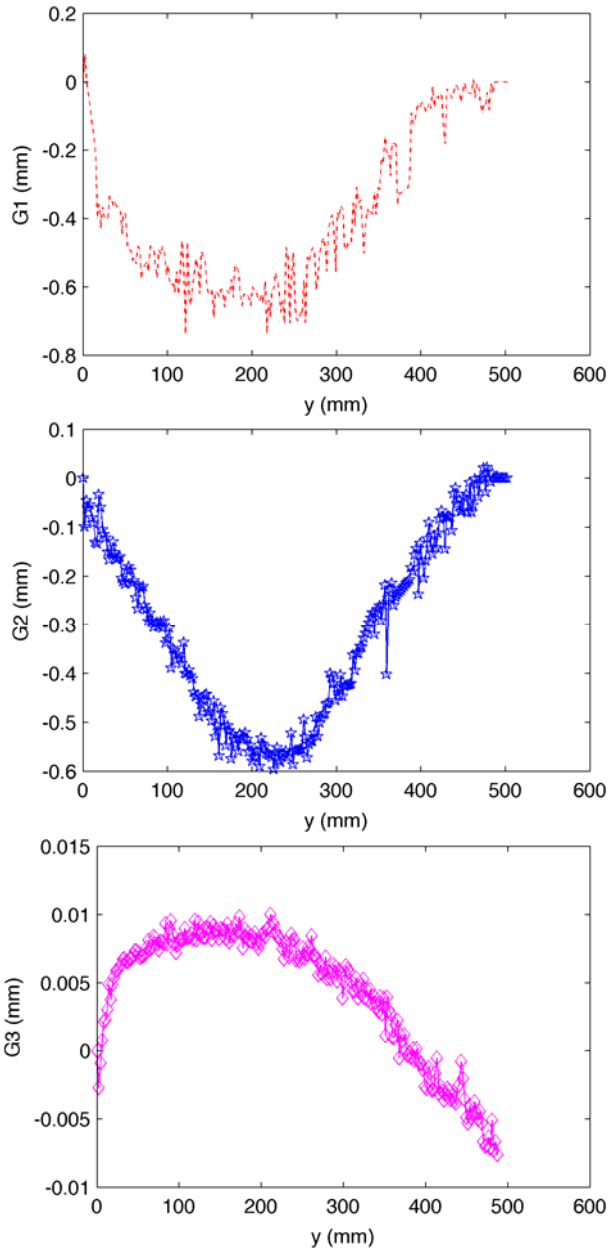

Figure 16 Typical G1, G2, G3 imperfections along the length

Type 1 (Local) and Type 2 (Distortional) Imperfections

Type 1 and 2 imperfections are estimated along the length as shown in Figure 17. The maximum values are summarized in Table 4. Maximum deviations typically occur near the ends of the specimen, as opposed to midspan. Given a nominal t of 1.37mm the mean $d2^{RF}/t=0.93$, and $d1/t=1.45$, which compares with approximately the 60^{th} percentile of measured d2 imperfections, and the 90^{th} percentile for d1 imperfections as reported by Zeinoddini and Schafer (2012).

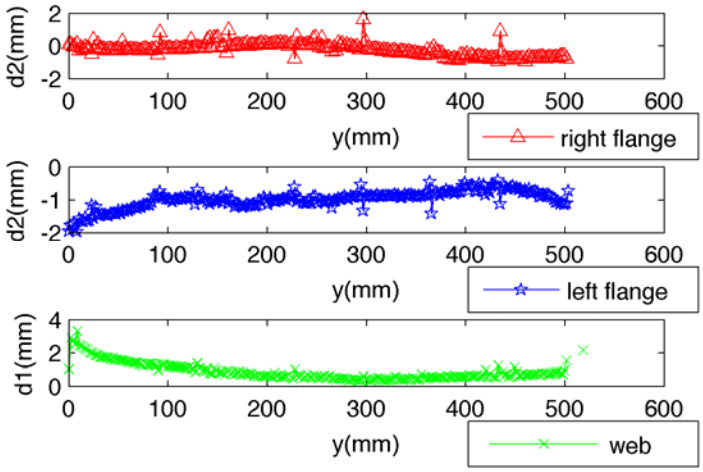

Figure 17 Typical Type 1 and 2 imperfections along the length

Table 4 Magnitudes of Type 1 and 2 imperfections

ID	$d2^{RF}$ (mm)	$d2^{LF}$ (mm)	d1 (mm)
1	1.64	-0.41	2.13
2	1.55	-0.73	1.76
3	0.76	0.49	4.49
4	0.87	0.32	1.48
5	2.23	0.95	2.24
6	-0.01	-5.78	1.88
7	0.96	0.74	1.14
9	0.90	0.06	1.61
10	1.41	0.33	1.49
11	2.51	-0.01	1.70
mean	1.28	-0.39	1.99
std. dev.	0.74	1.93	0.93

Dimension comparison between laser and manual measurement
Manual measurement of the same 10 specimens using digital calipers at three locations along the length as reported in Torabian et al. (2013) are compared to the mean laser measurements in Figure 18. The laser measurements are consistently smaller than the manual measurements. Relative differences among web height, right flange and left flange are 0.8%, 3.8%, and 2.3% respectively.

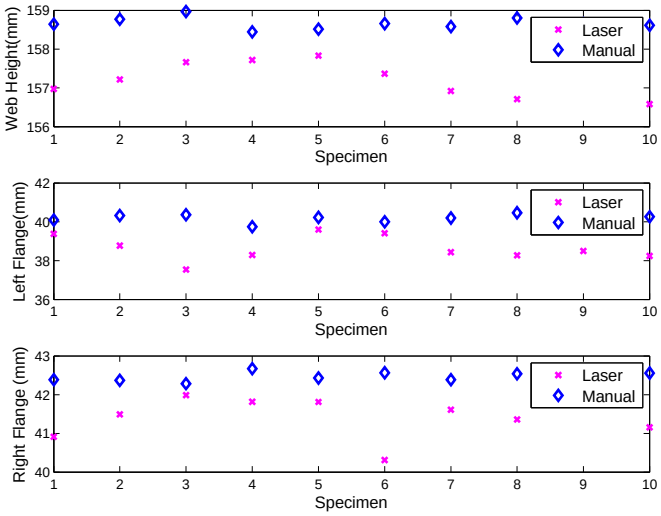

Figure 18 Comparison of mean dimensions across 10 specimens

Future Work

This paper is intended to show the potential for non-contact laser measurement of cold-formed steel members. Significant future work remains, including the following items. Perform additional benchmark studies. Provide definitive calibrations. Provide improved methods for removing scatter and other post-processing of the measured data. Implement the Phase II testing rig, which will obviate the need for the stitching performed herein and as a result increase the throughput and accuracy. Measure a variety of sections to fill out the imperfections database for use in better understanding cold-formed steel member imperfections and for better simulating such imperfections. Measure specimens under load and the resulting deformations in addition to initial imperfections. Use the developed data to better calibrate the design power spectral density functions proposed by Zeinoddini (2012).

Conclusions

Geometric imperfections are important for the strength and response of cold-formed steel members. A new imperfection measurement rig has been developed that utilizes a two-dimensional line laser on a translational stage to provide non-contact measurements of cold-formed steel members. The rig requires four separate passes to produce a full field measurement of a member. The four passes must be stitched together, and this is achieved through a two-step minimization process. The resulting three-dimensional point cloud provides a complete virtual model of the member. Ten nominally identical specimens are measured, stitched together, and then assessed. The resulting data provides a rich characterization of member dimension and member imperfections; further characterization is possible and desirable. The goal of the research is to develop a high throughput measurement device and significantly expand the available imperfection database for cold-formed steel members.

Acknowledgements

This work was partially funded by the National Science Foundation (NSF), Grant 1235196. Any opinions, findings, conclusions, or recommendations stated are those of the author(s) and do not necessarily reflect the views of the National Science Foundation.

References

Arbocz, J., & Hol, J. (1991). Collapse of axially compressed cylindrical shells with random imperfections. *AIAA Journal , 29* (12), 224702256.

Arbocz, J., & Williams, J. G. (1977). Imperfection survey on a 10-ft diameter shell structure. *AIAA Journal* , 949-956.

Chryssanthopoulos, M., & Poggi, C. (1995). Sotchastic imperfection modelling in shell buckling studies. *Thin-Walled Structures , 23* (1-4), 179-200.

Keyence Corporation. (2012). Retrieved 04 2014, from www.keyence.com

Koiter, W. T. (1967). *On the stability of elastic equilibrium.* NASA TT-F10.

Schafer, B. W. (1997). *Cold-formed steel behavior and design: analytical and numerical modeling of elements and members with longitudinal stiffeners.* Ph.D. Thesis, Cornell.

Sebek, R. W. (1981). *Imperfection surveys and data reduction of ARIANE interstages I/II AND II/III.* Delft University of Technology, Aerospace Engineering. thesis.

Singer, J., Abramovich, H., & Yaffe, R. (1979). Initial imperfection measurements of stiffened shells and buckling prediction. *21st Israel annual conference on aviation and astronautics. 17*, pp. 324-228. Israel Journal of Technology.

Torabian, S., Zheng, B., & Schafer, B. W. (2014). Experimental study and modeling of cold-formed steel lipped channel stub beam columns. *Proceedings of the Annual Stability Conference, Structural Stability Research Council.* Toronto.

Zeinoddini, V. M. & Schafer, B. W. (2011). Global Imperfections and Dimensional Variations in Cold-Formed Steel Members. *International Journal of Structural Stability and Dynamics, 11* (5).

Zeinoddini, V. M. & Schafer, B.W. (2012). Simulation of geometric imperfections in cold-formed steel members using spectral representation approach. *Thin-Walled Structure, 60 (2012) 105-117.*